Thin-Walled Structures 49 (2011) 1–12

Contents lists available at ScienceDirect

Thin-Walled Structures

journal homepage: www.elsevier.com/locate/tws

Mechanics of axial plastic collapse in multi-cell, multi-corner crush tubes

Ali Najafi, Masoud Rais-Rohani *

Aerospace Engineering Department, Center for Advanced Vehicular Systems, Mississippi State University, Mississippi State, MS 39762, USA

ARTICLE INFO

Article history:
Received 20 February 2010
Received in revised form
1 July 2010
Accepted 19 July 2010
Available online 1 September 2010

Keywords:
Crush tube
Energy absorption
Mechanics of crush
Multi-corner tube
Quasi-static crush

ABSTRACT

Quasi-static nonlinear finite element simulations are performed to study the energy absorption characteristics of axially crushed thin-walled aluminum tubes with different multi-cell, multi-corner configurations. By considering the kinematically consistent representation of plastic collapse as observed in the crush simulations, an analytical formula for the mean crush force is derived using the super folding element theory. In this model, the isotropic material is treated as rigid-perfectly plastic and the total internal energy is calculated by considering both bending and membrane deformation during the folding process. The simulation results show a strong correlation between the cross-sectional geometry and the crush response of the tubes. The analytical predictions for the mean crush force are compared with the FE results as well as other analytical models reported in the literature.

1. Introduction

In design of automotive structures, the desire for weight reduction (lightweighting) has to be balanced by the need for crashworthiness. Vehicle structural components such as the front rails play a crucial role in energy absorption management in frontal crash scenarios [1]. While the component has to be sufficiently stiff to limit intrusion distance, it has to accommodate sufficient amount of plastic deformation to attenuate the impulsive force and the associated acceleration transferred to the occupants. The energy absorption capacity of a rail depends not only on its material properties but also on its geometric configuration and mode of deformation. Besides their ease of manufacturing through the extrusion process, prismatic tube models are very suitable for the study of deep plastic collapse or the general mode of deformation under axial crush load, and as such, have received considerable attention for many years.

Early investigations of deep plastic collapse in thin-walled tubes made of ductile materials originated from the pioneering works of Alexander in 1960 [2] on cylindrical tubes and those of Wierzbicki and Abramowicz [3] and Abramowicz and Jones [4] on multi-corner tubes.

Through examination of the collapsing response of axially crushed single-cell rectangular tubes in laboratory experiments, Wierzbicki and Abramowicz [3] developed a self-consistent theory built upon the hypothesis that the plastic energy dissipated during the crush process can be related to the localized inextensional and extensional deformations observed at each corner and web region of the tube. They also assumed that as multiple folds develop during the progressive collapse, the folding distance or wavelength within each fold stays constant. Using a rigid-perfectly plastic isotropic material model, the average flow stress was related to plastic energy dissipation using the strain rate tensor, the Cauchy stress tensor, and the assumption of co-rotational yield condition. By dividing the rectangular cross-section into four identical two-flange (angle) sections and adding the contributions of the folding mechanisms at a representative corner element multiplied by the number of corners, they derived a closed form equation for the axial mean crush force that could be used to characterize energy absorption in rectangular tubes. The theoretical predictions were later modified and compared with data from laboratory experiments [4].

As an extension of their earlier work, Abramowicz and Wierzbicki [5] proposed a mixed folding mechanism model by combining quasi-inextensional and extensional modes of deformation observed in multi-corner tubes with arbitrary corner angles such as hexagonal and rhomboidal sections. By considering extensional, inextensional, and quasi-inextensional deformation mechanisms, Wierzbicki and Abramowicz [6] developed basic folding element (BFE) model for a more general theory for progressive collapse in single-cell, multi-corner tubes. These studies revealed that extensional deformation has a more dominant influence on the crushing of thick obtuse angle elements whereas the primary deformation mode for acute angle elements is the quasi-inextensional mode [7]. The resulting super folding element (SFE) model was described in terms of fifteen separate elements with characteristics of the deformable

* Corresponding author. Tel: +1 662 325 7294.
E-mail addresses: Ali@cavs.msstate.edu (A. Najafi), Masoud@ae.msstate.edu (M. Rais-Rohani).

0263-8231/$ - see front matter © 2010 Elsevier Ltd. All rights reserved.
doi:10.1016/j.tws.2010.07.002

elements described in terms of the three principal folding mechanisms: inextensional, quasi-inextensional, and extensional. The key aspect of SFE is the recognition of the formation and propagation of various hinge lines that define the boundaries of the constituent trapezoidal, toroidal, and cylindrical surfaces during the crushing process. They noted that for tubes with dissimilar corner angles, the fold wavelengths at the obtuse and acute corners can be distinctly different depending upon the difference in the angles.

Chen and Wierzbicki [8] studied the axial crush performance of multi-cell, multi-corner tubes with identical rectangular cells consisting of two- or three-member corners. They considered both hollow and foam-filled tube models. For simplicity, the kinematically admissible model of SFE [6] was replaced with a basic folding element to model both the membrane action, characterized by three extensional triangular elements near the corner line, and the bending action, modeled using three stationary hinge lines over each flange. By dividing the tube cross section into separate flange sections, and relating the fractional energy absorption of each flange to its length, thickness and assuming an average folding wavelength, they arrived at an analytical equation for the mean crush force.

Kim [9] applied the model of Chen and Wierzbicki [8] to multi-cell, multi-corner tubes with dissimilar cells having right-angle corners. Zhang and Cheng [10] also adopted the approach of Chen and Wierzbicki [8] to derive an analytical equation for the mean crush force for multi-cell rectangular tubes with four to nine identical rectangular cells. However, they divided the cross section into separate 2-, 3- and 4-flange corners, and measured the contribution of each corner type to plastic energy dissipation through membrane action. The resulting analytical equation for the mean crush force assumes an average wavelength for the dissimilar folds developed at the corners.

Although both static and dynamic tests have been used to measure the collapse response of multi-corner crush tubes, the effect of dynamic load on the material properties is often ignored in analytical solutions. Langseth and Hopperstad [11] performed extensive experiments on different heat-treated square aluminum tubes under both static and dynamic loads, and showed that under static loading, most of the mode shapes are symmetric whereas in dynamic cases, the mode shapes tend to vary during the crush deformation. DiPaolo et al. [12] and DiPaolo and Tom [13] conducted a series of controlled experiments focused on the symmetric quasi-static axial crush response of welded stainless steel square tubes. They first investigated different control methods in the form of tube end constraints and collapse initiators (triggers) to control the so-called configuration response (combination of collapse geometry and the shape of the load–displacement curve). This was then followed by the examination of the effects of alloy composition and microstructure on the configuration response. Their results showed that the combination of greater carbon content and smaller grain size enhanced both the peak crush load as well as energy absorption for the secondary fold formation.

The development of nonlinear finite element analysis (FEA) codes such as LS-DYNA, made it possible to analyze the crash phenomenon [14–18] as a non-smooth, highly nonlinear problem based on the explicit time integration technique [19]. Most of the element models used in these codes were originally developed by Hughes [20,21] and Belytschko et al. [19] with subsequent modifications aimed at correcting the problem of zero energy (hourglass modes) and enhancing the computational efficiency.

In the case of contact formulation, the kinematic constraint, penalty and distributed parameter methods are often used for rigid body and self-contact calculations [22,23]. To include material nonlinearity, many of the previous studies have used classical elastic–plastic models with kinematic and/or isotropic hardening behavior [24].

One way to control the crush zone and plastic deformation of tubes is through the design of tube cross-section. The extrusion process makes it possible to easily manufacture various prismatic tubes with multi-cell, multi-corner cross-sectional configurations. Previous studies [8–10,25–27] show that multi-cell profiles with two or more rectangular cells can enhance the energy absorption capacity of crush tubes. Specifically, Chen and Wierzbicki [8] show that the addition of interior walls can increase the specific energy absorption (SEA) by approximately 15% in comparison to the single-cell model.

Among all the multi-cell models considered in the previous analytical studies, those in Kim [9] appear to be the most complex. Although more complicated multi-cell models have appeared in the literature, the theoretical analysis was replaced by either FE solutions [17,18] or a surrogate model developed using the response surface methodology [28,29].

While there have been many studies on multi-cell tubes, very few have considered the energy absorption characteristics of multi-corner, multi-cell tubes with non-rectangular or dissimilar cell geometry. In this study, the mechanics of plastic collapse in single-cell and multi-cell tubes is investigated using nonlinear FEA. Based on the deformation modes observed in the FE simulations and the theoretical foundation provided by the earlier research mentioned above, an analytical equation for the mean crush is developed with the results compared with those of FE solutions.

The remaining portion of the paper is organized as follows: Section 2 describes the FE model and associated nonlinear simulations. The analytical approach is presented in Section 3, followed by the discussion of results and the concluding remarks in Sections 4 and 5, respectively.

2. Quasi-static finite element simulations

2.1. Tube models

The tube models of interest in this paper are prismatic with cross-sectional shapes shown in Fig. 1. They generally possess two- or multi-member junctions (corners) with acute or obtuse angles. The selected models generally show a square inner tube (d_i=40 mm) connected to a square outer tube twice its size (d_o=80 mm). The multi-cell tube in all models has a length of 400 mm and a constant wall thickness (t=2 mm). The distinguishing feature among the four models in Fig. 1 is the way the inner and outer tubes are connected together to form the multi-cell geometry. The connecting webs create corner-to-corner (C2C), corner-to-web (C2W), web-to-corner (W2C), and web-to-web (W2W) attachments in these models. Although the shape and size of the inner and outer tubes are identical in all four models, there is a slight weight difference due to minor variation in width dimensions of the connecting webs. For reference purposes, the performance of multi-cell models is compared with that of a square tube of approximately similar energy absorption level with d=80 mm and t=4 mm.

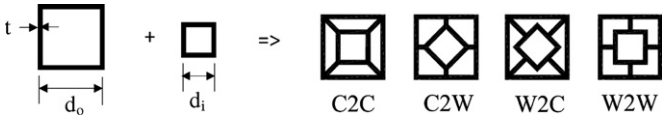

Fig. 1. Cross-sectional geometry of multi-cell, multi-corner tube models.

2.2. Material model

All models in this study are made of AA6060-T6 aluminum alloy ($E=70$ GPa, $v=0.3$, and $\rho=2.7e-6$ kg/mm^3). The material behavior is expressed in terms of true stress–true strain curve, which is extracted from a tension test up to the ultimate stress point [30]. Since no failure or damage is defined in this simulation, the stress–strain curve is extended in a perfectly plastic manner beyond the ultimate stress point as shown in Fig. 2. Using the J_2 plasticity model with multi-linear isotropic hardening law, the stress–strain curve is treated as piecewise linear. The rate sensitivity effect is ignored in this analysis as the material is reported to be rate insensitive and the loading is assumed to be quasi-static.

2.3. Simulation setup

In the quasi-static FE simulations, the tube is held fixed at its base and a linear incremental displacement is applied at its free end as shown in Fig. 3. All FE models use Hughes-Liu (continuum based) shell elements [31,32]. An element mesh density study was performed to find a suitable element size for the models investigated. A subsequent examination showed that energy absorption can be accurately estimated by using only three integration points (NIP=3) through the shell thickness. Because of the high element distortion, zero energy deformation or hourglass energy [19,31,32] was also checked. Results showed a very small hourglass energy ($<2\%$ of the total internal energy generated due to load).

The contact friction coefficient between the rigid wall and the tube is set at 0.3 to prevent slippage due to numerical error between the two surfaces (wall force). To prevent element–element penetration resulting from excessive deformation, a frictionless self-contact condition is defined on both inner and outer surfaces of each element. The FE models used here are developed using the ANSYS-preprocessor with FEA simulations performed using transient dynamic nonlinear explicit FE code LS-DYNA (double precision).

All simulations are conducted on a 16-node cluster with dual-core AMD Opteron 2218 processors (2.6 GHz) and 8 GB of memory. The post-processor LSPREPOST is used for visualization and data analysis. To filter out noise in load history results, the SAE type filtering with the frequency of 60 Hz is used. The termination time of 400 ms is used for quasi-static analysis resulting in the 1 m/s constant velocity of axial loading on the tube throughout the simulation.

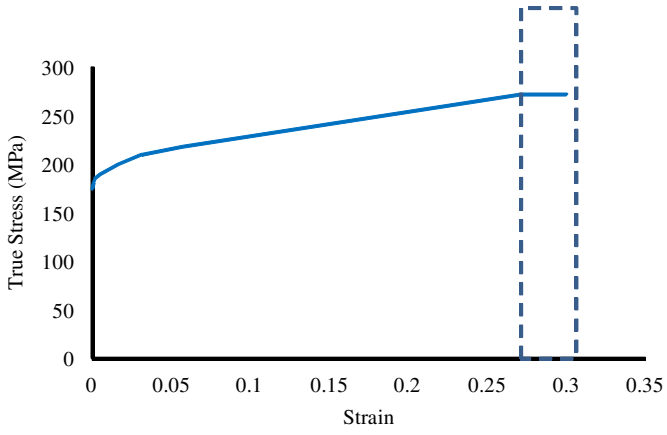

Fig. 2. Stress–strain relationship in piecewise linear plasticity model used in FE simulations.

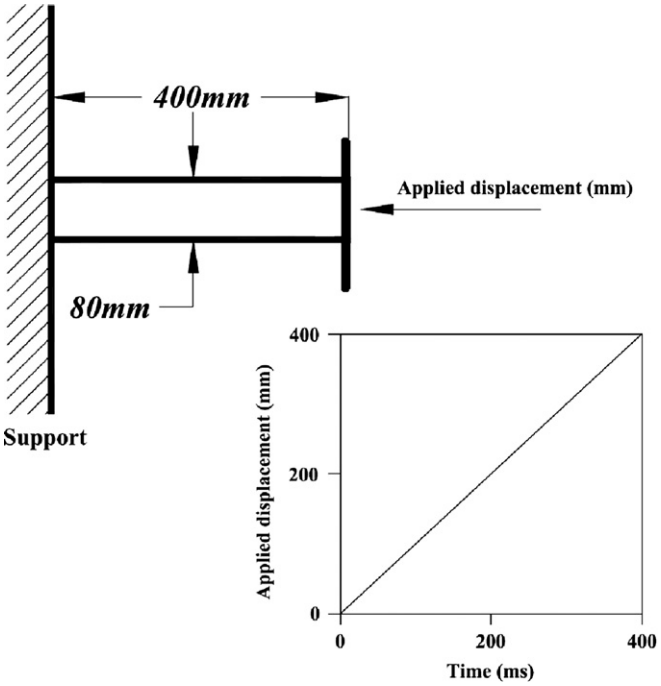

Fig. 3. Quasi-static model setup.

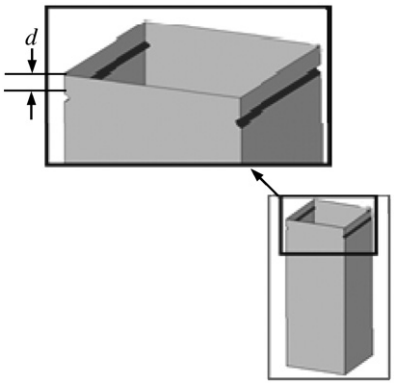

Fig. 4. Indentation trigger mechanism.

A small indentation on two opposite walls of the external tube near its free end as shown in Fig. 4 is used as a trigger mechanism. As reported in the literature [9], we found that an indentation trigger mechanism can lower the initial peak crush force, induce a stable progressive collapse, and prevent the global buckling of the tube while it is crushed.

2.4. Crush response of a square tube

Since the collapse behavior is heavily influenced by the deformation of corner regions, the collapse response of a simple square tube is used as reference. In general, the folding mechanism in a two-flange corner region involves extensional, quasi-extensional, and quasi-inextensional modes of deformation [4]. Using the description presented by Abramowicz [7], the folding deformation can be expressed in terms of asymmetric and symmetric corner elements as shown in Fig. 5. Although the symmetric mode, with all corner regions deforming as in Fig. 5b, is computationally possible, it has not been observed in physical crush experiments.

We performed a series of FE simulations to model the crush response of a square tube with an isothermal rate insensitive piecewise linear plasticity model as shown in Fig. 2, and found the crush mode to be highly dependent on the trigger mechanism and the loading rate. By adjusting the location of indentation trigger mechanism under quasi-static loading, we were able to find both the symmetric and asymmetric modes as shown in Fig. 5.

As noted in Wierzbicki and Abramowicz [6] and Abramowicz and Jones [4], symmetric collapse mode involving symmetric and asymmetric elements includes a cylindrical surface created from the horizontal hinge lines caused by inextensional deformation, inclined hinge lines forming inextensional deformation through the conical surface, and a toroidal surface that has quasi-inextensional deformation. In the toroidal surface, two bending deformations are present [33]. The double bending action is due to the cylindrical surface formed through the formation of inclined hinges combined with a global bending due to cylindrical formation of horizontal hinge lines. A toroidal surface is formed because of the subsequent bending.

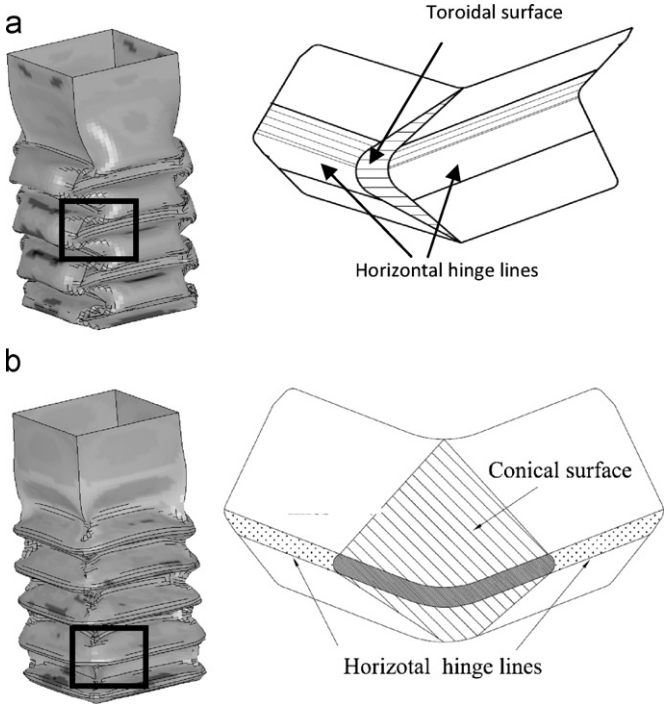

Fig. 5. (a) Asymmetric and (b) symmetric (extensional) elements resulting in symmetric collapse deformation.

Symmetric extensional collapse mode involving only symmetric elements includes horizontal and inclined hinge lines along with a conical surface that has extensional deformation. Whereas in symmetric quasi-inextensional collapse mode involving only asymmetric element the major part of energy is dissipated through quasi-inextensional deformation of the toroidal surface, in the symmetric elements or extensional deformation, energy dissipation is mainly due to the extensional deformation of the conical surface.

The cut view in Fig. 6 illustrates the progression of the symmetric collapse mode in a square tube involving only asymmetric elements. The folds start to appear in succession as the applied displacement (load) is increased. Each fold maintains its configuration as the next fold starts to develop. A load peak appears as a horizontal hinge line begins to form. In symmetric elements, the toroidal surface controls the crush force while folds continue to accumulate with the surface of adjacent folds contacting each other as shown in Fig. 6F. This phenomenon has been captured in FE simulations by defining self-contact in such a way that no node can penetrate any of the tube elements. The presence of self-contact preserves each crushed fold in such a way that the force required to increase deformation is greater than that for forming a new fold. At this point, the folded region behaves as a bulk rigid structure such that any further deformation will be impossible unless there is enough room for new folds to develop.

Owing to the formation of the toroidal/conical surface and the cylindrical hinge lines, the crush distance is not equal to the tube length. Subsequently, once multiple folds are developed over the entire length, the amount of force required to deform the tube increases substantially. This is known as *locking phenomenon*. The effective crush distance is calculated by considering the accumulation of folds up to the locking point. The internal dissipated energy is calculated from crush force versus crush distance curve up to this point, and the overall mean crush force is found by dividing this calculated energy by the effective crush distance.

2.5. Crush response of multi-cell, multi-corner tubes

The collapse modes of the multi-cell, multi-corner tube models are shown in Fig. 7. All models undergo a stable progressive collapse with repeated folding deformation that extends to nearly 65% of the length in all configurations. In C2C and C2W configurations, the effective crush distance is longer than that of W2C and W2W configurations. Therefore, the length of the rigid bulk in W2W and W2C configurations is greater than that in C2C and C2W.

The cut views of the crushed multi-cell tubes are shown in Fig. 8. The figure reveals a more complicated folding pattern than

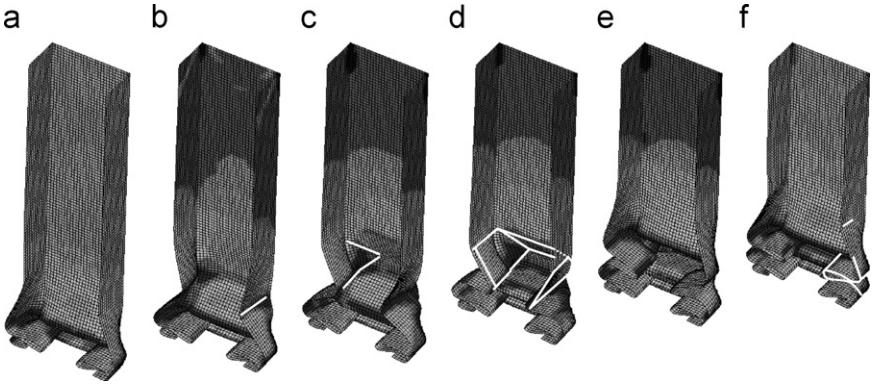

Fig. 6. Folding progression in a square tube under quasi-static axial compression.

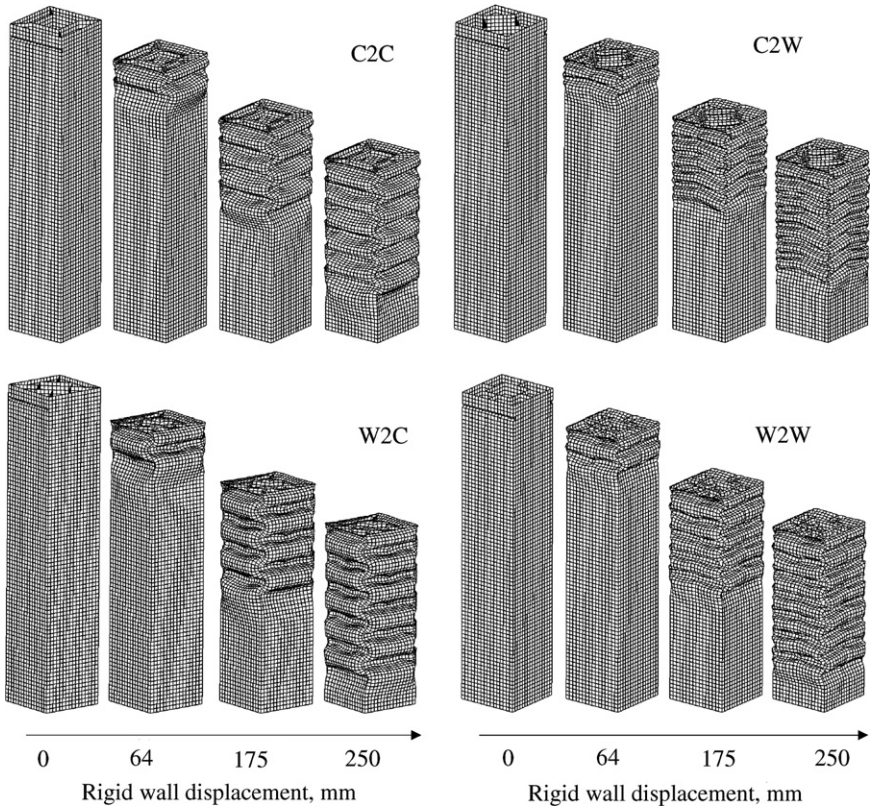

Fig. 7. Progressive collapse of different multi-cell, multi-corner tube models (deformation scale factor=0.7).

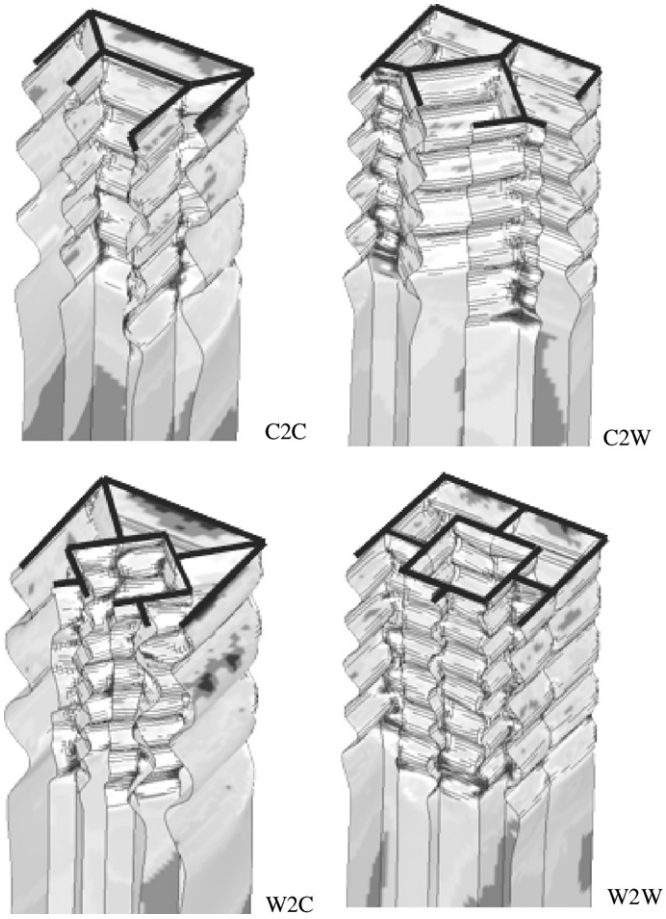

Fig. 8. Cut views revealing the deformation patterns in different multi-cell tubes.

that observed previously in single-cell tubes. The complex folding pattern stemming from multi-corner configuration (i.e., the number and angles of members joined at each corner) depicts the interaction of large number of folds in the inner, outer, and connector walls and is indicative of a larger portion of the structure participating in the plastic deformation. Having the same wall thickness, the wall dimensions cause a difference in the folding height in the inner, outer, and the connector walls. It can be seen that the folding patterns in the C2C and W2W configurations are more uniform as the number of folds in the inner and outer tube walls are approximately equal.

The close-up views of the folding patterns in Fig. 9 show that the three-member corners with obtuse, acute, and right angles can have different deformation patterns. For example, Fig. 9a shows that the three-member corners with obtuse angles deform under the symmetric mode shape. The difference in deformation patterns of the two- and three-member corners become important in the development of an analytical equation for the mean crush force, as will be discussed later.

2.6. Energy absorption in single- and multi-cell tubes

Fig. 10 shows the plots of crush force versus crush distance for the multi-cell tubes. In each case, the crush response is compared with that of the square tube model with an equivalent cross-sectional area. The thickness of the square tube is twice that of the multi-cell models so that its mean crush force is close to that of the multi-cell tubes. The range of the crush force fluctuation and the slope of the load–displacement curve in multi-cell tubes are smaller than those of the square tube. The load–displacement behavior of multi-cell tubes shows that the number of folds cannot be easily identified from the load–displacement curve.

Another characteristic of the multi-cell tubes is that their effective crush distance is shorter than that in the square tube.

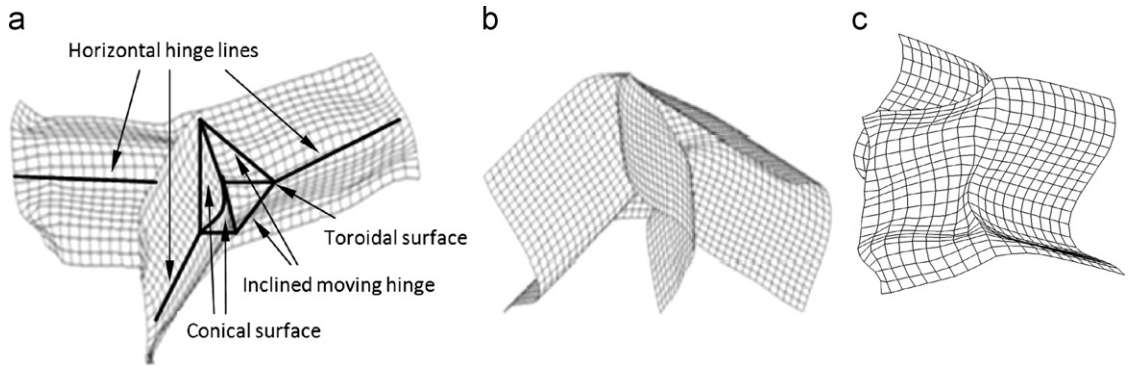

Fig. 9. Plastic deformation pattern at three-member corners with (a) obtuse, (b) acute, and (c) right angles.

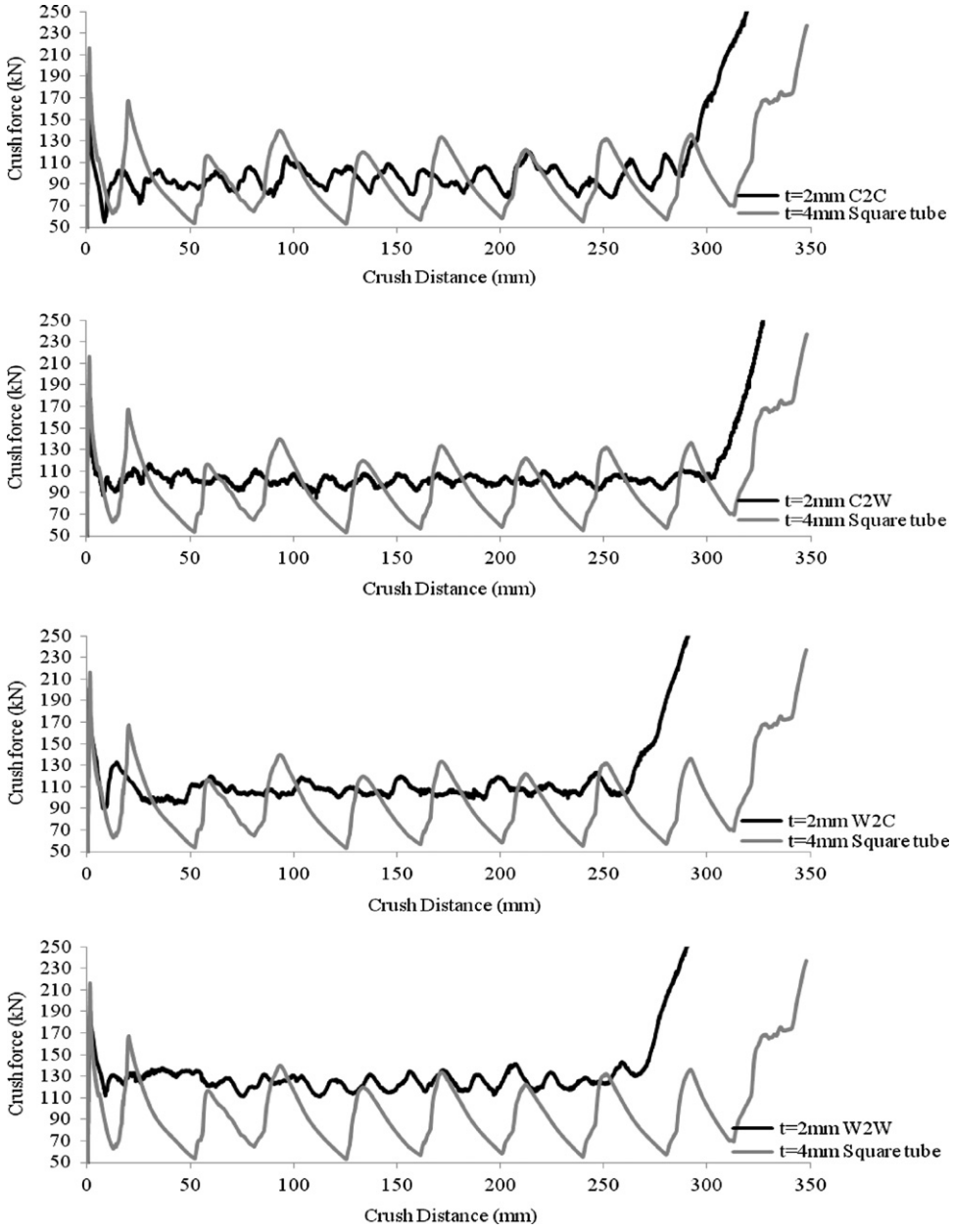

Fig. 10. Crush force versus crush distance for different tube models.

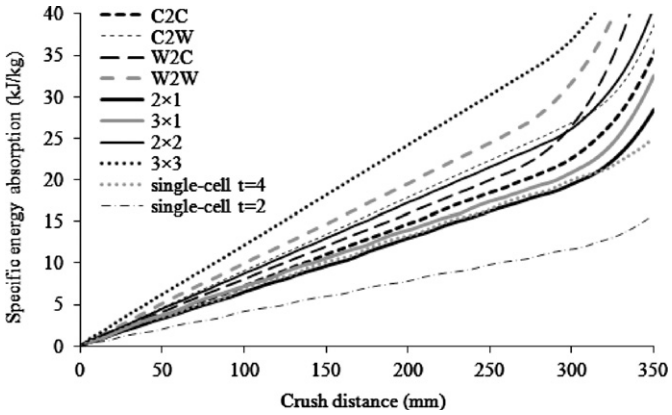

Fig. 11. Comparison of specific energy absorption for different tube models.

This shorter effective crush distance is primarily due to the locking of external and internal folds by the folding of connector walls that do not allow the complete folding of the inner and outer walls.

The specific energy absorption (SEA) of a component is defined as the ratio of absorbed energy to the structural mass. In Fig. 11, the SEA values for different multi-corner configurations are compared as a function of crush distance. The models labeled by $a \times b$ represent multi-cell tubes with a rectangular cells in one direction and b in the other. The curves show a linear trend up to the point where locking begins. The total SEA for each configuration is calculated up to the initiation of locking. Amongst the four multi-cell models considered here, configuration W2W has the highest and C2C the lowest SEA value. The mean crush force of C2W is very close to that of W2C configuration, but due to their slight weight difference, the SEA and effective crush distance of C2W are higher than those in W2C configuration.

3. Analytical modeling of crush response

We are extending the methodology and formulation of kinematic based solution of crushing response in single-cell, multi-corner sections developed by Wierzbicki and Abramowicz [6] to multi-cell, multi-corner sections with acute and obtuse angles. Since progressive axial crush of thin-walled prismatic tubes with associative materials is characterized by the presence of highly localized zones of plastic flow, a similar approach as the upper-bound theorem [34,36] is used for analyzing their energy absorption behavior.

The upper-bound theorem can only be used to determine the initial collapse mechanism, the initial load or its bounds. However, the components designed for energy absorption are usually expected to experience large plastic deformation under external loads.

The main elements of this analysis include: (1) the energy balance equation, (2) identification of kinematically admissible deformation including geometric parameters that control the collapse process, (3) proper constitutive assumption to combine the work conjugate variables of strain type variables present while defining kinematically admissible deformation, and (4) applying the extremum condition on the energy balance equation to optimize the geometric parameters based on energy minimization.

A displacement/velocity field is kinematically admissible if it is continuous in the structure, satisfies the velocity/displacement boundary conditions, and the external force does positive work on this displacement/velocity field [35]. Combining the kinematically admissible deformation with constitutive equation gives the internal energy equation for each localized region, and the contribution of unknown parameters is captured by applying the extremum condition to the energy balance equation.

The energy balance rate equation is generally expressed as

$$\dot{W}_{ext}(\dot{u}) = \dot{E}_{\text{int}}^{Total}(\dot{\varepsilon}) \tag{1}$$

where $\dot{W}_{ext}(\dot{u})$ is the rate of external work and $\dot{E}_{\text{int}}^{Total}(\dot{\varepsilon})$ is the rate of energy dissipation in the plastically deformed regions. Eq. (1) is analogous to the work-energy balance between the internal energy and work done by the applied load.

In the case of axial crush analysis, the rate of external work is calculated based on the instantaneous crushing force P and the axial crush velocity $\dot{\delta}$ given as

$$\dot{W}_{ext}(\dot{u}) = P\dot{\delta} \tag{2}$$

The right hand side of the energy balance in Eq. (1) should contain the total energy dissipation contribution of the whole structure. For this purpose, we need to identify the energy absorption behavior of each localized region separately and sum up their individual contributions. In general, for shells made of rigid-perfectly plastic isotropic materials that experience plastic deformation in localized regions, the rate of internal energy dissipation is divided into continuous and discontinuous velocity fields [7,8] represented by

$$\dot{E}_{int} = \int_S (M_{\alpha\beta}\dot{\kappa}_{\alpha\beta} + N_{\alpha\beta}\dot{\varepsilon}_{\alpha\beta})dS + \sum_{i=1}^{m}\int_{L^i} M_o^i \dot{\theta}^i \, d\ell^i \tag{3}$$

where S defines the extent of continuous plastic deformation, L^i is the length of the ith hinge line, and m is the total number of stationary or moving hinge lines. In the continuously deforming zones, the bending moments $M_{\alpha\beta}$ and membrane forces $N_{\alpha\beta}$ are the conjugate generalized stresses for the components of the rotation rate tensor $\dot{\kappa}_{\alpha\beta}$ and extension rate tensor $\dot{\varepsilon}_{\alpha\beta}$, respectively, with M_o^i representing the fully plastic bending moment per unit length and $\dot{\theta}^i$ representing the rotation rate of the hinge line.

In the SFE model of Wierzbicki and Abramowicz [6] as shown in Fig. 12, the collapse response of single-cell, multi-corner tubes is treated as a progressive phenomenon with each fold defined in terms of the fold height H, the toroidal surface curvature b, the corner angle θ, and the wall thickness t. The contribution of each localized region to the internal energy can be derived based on Eq. (3). Depending upon the corner angle, energy contribution of the two-flange corner sections can be represented by four types of localized regions as shown in Fig. 12. The combination of three localized regions can form two basic mode shapes (symmetric and asymmetric) that are predominantly seen in both physical experiments and FE simulations [7].

The asymmetric corner element that is dominant in acute and right corner angles contains toroidal surface, as well as inclined and horizontal hinge lines (Fig. 5a) whereas the symmetric corner element that is dominant in obtuse corner angles is comprised of

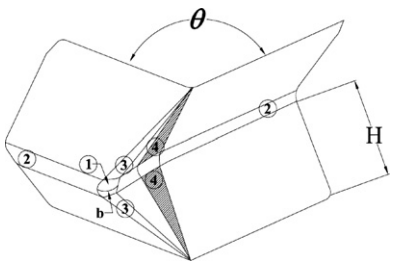

Fig. 12. The collapse geometry of SFE [6].

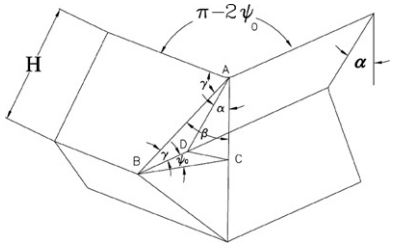

Fig. 13. Angle parameters used in energy absorption contribution equation.

conical surface and horizontal hinge lines (Fig. 5b) [7]. Defining pure mode shapes in corners gives more flexibility to develop an analytical equation for the mean crush force since the switching parameter [6,7] that defines the boundary between symmetric and asymmetric deformation modes is assumed to be known.

The basic geometry of the four fold lines in asymmetric deformation is presented in Fig. 13. The initial geometry of this asymmetric mode shape is defined by the element height $2H$, total width C, and the corner angle $\pi-2\psi_0$. The geometry in the current configuration can be expressed via either crush distance δ or the angle of rotation of tube side α [5–7].

The energy absorption in each of the localized regions including the toroidal surface E_1, horizontal hinge line E_2, and inclinded hinge lines E_3 are calculated based on the following equations, where the upper limits in Eqs. (4) and (6) have been set to $\pi/2$ to capture the asymmetric element:

$$E_1 = \frac{16M_0Hb}{t}\left[\frac{\pi}{(\pi-2\psi_0)\tan\psi_0}\right]\int_0^{\pi/2}\cos\alpha\left\{\sin\psi_0\sin\left(\frac{\pi-2\psi_0}{\pi}\beta\right)+\cos\psi_0\left[1-\cos\left(\frac{\pi-2\psi_0}{\pi}\beta\right)\right]\right\}d\alpha \tag{4}$$

$$E_2 = 2M_0C\left(\frac{\pi}{2}\right) \tag{5}$$

$$E_3 = \frac{2M_0H^2}{b\tan\psi_0}\int_0^{\pi/2}\frac{\cos\alpha}{\sin\gamma}d\alpha \tag{6}$$

The energy absorption contributions in the localized regions associated with the symmetric element including conical surfaces and horizontal hinge lines are calculated as

$$E_4 = \frac{2M_0H^2\tan\psi_0}{t}\int_0^{\pi/2}\left(\frac{\sin2\alpha}{1+\tan^2\psi_0\sin^2\alpha}\right)d\alpha \tag{7}$$

$$\gamma = \tan^{-1}\left(\frac{\tan\psi_0}{\sin\alpha}\right) \tag{8}$$

$$\beta = \tan^{-1}\left(\frac{\tan\alpha}{\sin\psi_0}\right) \tag{9}$$

where the angles γ and β, as shown in Fig. 13, are defined in *ABD* and *ABC* planes, respectively.

It is worth noting that in E_2, E_3, and E_4, the energy contribution of each localized region should be doubled while considering the two-flange corner elements.

The folding patterns in Fig. 9 show that the three-member corners are comprised of the aforementioned localized regions. By incorporating the energy dissipation contributions of each corner region, the mean crush force of multi-cell, multi-corner tubes can be calculated.

Three types of three-flange elements, identified as types I and II and T in Fig. 9 are considered. Table 1 shows the distribution of localized regions in each corner element of the multi-cell models (C2C, C2W, W2C, and W2W). Type-I element is a combination of an acute and a right angle while type-II is a combination of an obtuse and a right angle. Simple T elements that are present in models C2W, W2C, and W2W are treated as a combination of two right-angle corners (Fig. 14).

Table 1
Distribution of corner elements in multi-cell, multi-corner tubes.

Model	2-flange elements	3-flange elements (type-I)	3-flange elements (type-II)	3-flange elements T-shape
C2C	0	4	4	0
C2W	4	0	4	4
W2C	4	4	0	4
W2W	8	0	0	8

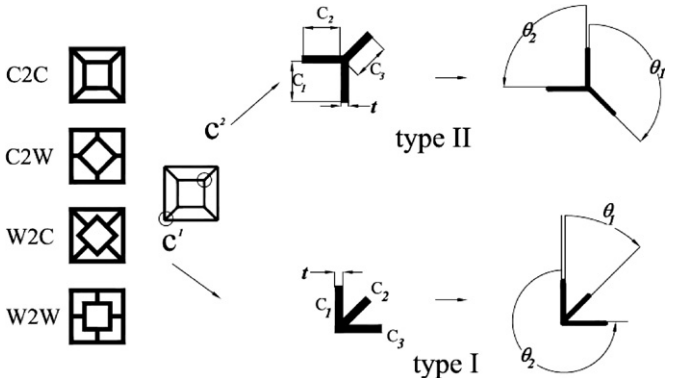

Fig. 14. Alternative cross-sectional models and geometric parameters.

The energy contributions for each corner type, as identified from FE analysis in Fig. 9, are based on the deformation pattern observed in the localized regions of the aforementioned basic folding modes by considering the corner angles and the flange dimensions (Fig. 13) [39]. Table 2 summarizes the number of localized regions in each corner configuration along with the corresponding energy contribution. During deformation, the continuity condition imposed onto the common corner lines [7] creates a mixed mode response that is considered in the method presented in this study. Since the angle between flanges affects the energy absorption of toroidal and conical surfaces, the energy contribution of each localized region is calculated individually as summarized in Table 2.

In this analysis, the material is assumed to be rigid-perfectly plastic, which considers the incipient plastic flow. Therefore, the material can be characterized by a single parameter (i.e., flow stress) assuming a uniform strain over the entire localized region. The calculation of energy-equivalent flow stress is one of the major sources of discrepancy between the mean crush force calculated from the analytical equation and that found experimentally [37]. Although in modern SFE formulation the Baushinger effect is included, in the present study, this effect together with those associated with softening and failure or damage is ignored.

Power law is widely used for energy-equivalent flow stress calculation because of its good performance and simplicity. The energy-equivalent flow stress for stretching and bending deformation are simplified to the following equations:

$$\sigma_0^{stretching} = \frac{\sigma(\varepsilon_i)}{n+1}, \quad \sigma_0^{bending} = \frac{2\sigma(\varepsilon_i)}{(n+1)(n+2)} \tag{10}$$

where $\sigma(\varepsilon_i)$ is the stress corresponding to the maximum strain developed in each localized region [37]. It can be shown that the energy-equivalent flow stress values for bending and extension

Table 2
Localized regions and associated energy equations.

Localized region	Toroidal surface	Horizontal hinge line	Inclined hinge lines	Conical surface	Energy equation
2-flange	1	2	2	0	$E_{int}=E_1(\pi/2)+\sum_{i=1}^{2}E_2(C_i)+2E_3(\pi/2)$
T-shape	1	3	2	2	$E_{int}=E_1(\pi/2)+\sum_{i=1}^{3}E_2(C_i)+2E_3(\pi/2)+2E_4(\pi/2)$
Type-I	1	3	2	2	$E_{int}=E_1(\pi/2)+\sum_{i=1}^{3}E_2(C_i)+(E_3(\pi/2)+E_3(3\pi/2))+(E_4(\pi/2)+E_4(3\pi/2))$
Type-II	2	3	4	2	$E_{int}=(E_1(\pi/4)+E_1(\pi/2))+\sum_{i=1}^{3}E_2(C_i)+2(E_3(\pi/4)+E_3(\pi/2))+(E_4(\pi/4)+E_4(\pi/2))$

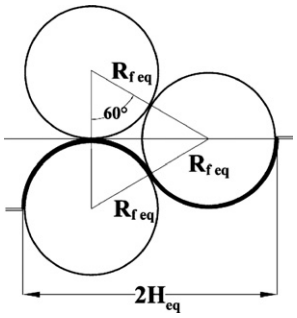

Fig. 15. Formation of folds for crush distance calculation in equal-size lobes.

are close considering the average value of flange sizes. For simplicity, the energy-equivalent flow stress in different regions of multi-cell, multi-corner tubes is assumed to be the same.

The mean crush force for multi-cell, multi-corner models C2C through W2W can be obtained by adding the contribution of each individual corner elements resulting in a closed form formula for the mean crush force expressed as

$$P_m=\frac{1}{2\chi H_{eq}}\sum_{j=1}^{n_e}N_jE_{int}^j \tag{11}$$

where N_j represents the number of each distinct corner elements from Table 1 with separate contributions to the total energy absorption of the tube, and n_e represents the number of element types present in the cross-section. Since Eq. (11) is based on a single value for equivalent projected fold height, H_{eq}, the effective crush distance is defined as $\delta_{eff}=\chi(2H_{eq})$. In the case of complete contact, where both faces of non-deformed components are collapsed completely on each other ($\chi=1$), experimental and numerical observations show that the folds are not in a plane surface and there is a curvature associated with this distance. Abramowicz [33] showed that the factor χ varies within the range of 0.60–0.75% for linear strain hardening materials in single-cell square tubes. FE simulation showed that the radius of the inward lobe is half of the radius of the outward lobe in the medium thickness single-cell tubes whereas the radii of the inward and outward lobes in each wall of the multi-cell tubes are equal (Fig. 15). Considering the averaging scheme used for the mean crush force calculation, the ratio of the effective crush distance and equivalent projected fold length ($2H_{eq}$) can be calculated from Fig. 15 to be

$$\chi=\frac{\delta_{eff}}{2H_{eq}}=1-\frac{x_{eff}}{2H_{eq}}=1-\frac{R_{feq}}{(\sqrt{3}+2)R_{feq}}=\sqrt{3}-1=0.73 \tag{12}$$

Here, we have two kinematic parameters that should be identified to calculate the mean crush force. Due to the constraint that has already been imposed on the set of kinematically admissible deformation, the boundary conditions, initial conditions, and loading are automatically satisfied. It can be concluded that the extremal values of the kinematically admissible parameters $\{H,b\}$ can be derived from the minimization of the mean crush force as

$$\frac{\partial P_m}{\partial H_{eq}}=0,\quad \frac{\partial P_m}{\partial b}=0 \tag{13}$$

The existence of this optimum path is shown by Hill [38] for the theory of plastic collapse, and was proven for axial crush [34]. Following the minimization condition in Eq. (13) for H and b, the equivalent b and H for multi-cell, multi-corner elements can be obtained as

$$b_{eq}=-\frac{t\beta}{4\lambda}-\frac{\xi}{4\sqrt{3}+\frac{1}{2}\zeta} \tag{14}$$

$$H_{eq}=\frac{1}{t\eta}\left(\frac{t^2\beta^2\gamma}{4\lambda^2}+\frac{\sqrt{3}t^3\beta^3\gamma}{8\lambda^3\xi}+\frac{1}{8\sqrt{3}\lambda}t\beta\gamma\xi-\frac{1}{4\lambda}t\beta\gamma\zeta-\frac{1}{4\sqrt{3}}\gamma\xi\zeta\right) \tag{15}$$

where

$$\xi(t,C,m,\kappa)=\sqrt{\frac{3t^2\beta^2}{\lambda^2}-\frac{162^{1/3}3^{2/3}Ct^3\eta^2(\mu_1+m\mu_2)}{\kappa}+\frac{22^{2/3}3^{1/3}\kappa}{\gamma^2\lambda}} \tag{16}$$

$$\kappa(t,C,m)=(-9Ct^5\beta^2\gamma^4\eta^2(\mu_1+m\mu_2)+\sqrt{3}\sqrt{C^2t^9\gamma^6\eta^4(\mu_1+m\mu_2)^2(27t\beta^4\gamma^2+256C\eta^2\lambda^3(\mu_1+m\mu_2))})^{1/3} \tag{17}$$

$$\zeta(t,C,m,\xi)=\sqrt{\frac{t^2\beta^2}{2\lambda^2}+\frac{4(2/3)^{1/3}Ct^3\eta^2(\mu_1+m\mu_2)}{\kappa}-\frac{\kappa}{2^{1/3}3^{2/3}\gamma^2\lambda}+\frac{\sqrt{3}t^3\beta^3}{2\xi\lambda^3}} \tag{18}$$

where the constants are specified in Table 3.

Substituting the terms in Eqs. (14) through (18) into Eq. (11) gives the general analytical equation for the mean crush force of multi-corner, multi-cell tubes. This equation is similar to the general form for single-cell tubes [6] and can be expressed as

$$P_m=\frac{\sigma_0 t}{\chi b_{eq}H_{eq}}\left(Ab_{eq}^2H_{eq}+BH_{eq}^2t+Kb_{eq}H_{eq}^2+Fb_{eq}Ct+Gb_{eq}mCt\right) \tag{19}$$

where C is the internal tube flange length, m is the ratio of external tube ($m=2$) flange by internal tube flange length and $\chi=0.73$ based on Eq. (12). Other constants for each configuration are listed in Table 3.

4. Results and discussion

The curves in Fig. 16 illustrate the variation of the mean crush force with changes in wall thickness as predicted by the analytical equation for the four multi-cell, multi-corner tube models. The FE

Table 3
Constants in Eqs. (9)–(14).

	C2C	C2W	W2C	W2W
μ_1	1.8403	−0.7623	−189.7430	10.6814
μ_2	10.7261	20.1508	604.0790	63.4602
λ	0.6582	1.1503	49.3361	14.4686
β	34.2118	86.7882	1101.8800	367.2940
γ	9.2457	17.9513	12.5951	20.1101
η	8.5529	10.8485	3.4434	5.7390
A	9.2457	17.9513	25.1902	40.2201
B	8.5529	10.8485	6.8868	11.4779
K	0.1645	0.1438	0.3084	0.4521
F	0.4601	−0.0953	−1.1859	0.3338
G	2.6815	2.5189	3.7755	1.9831

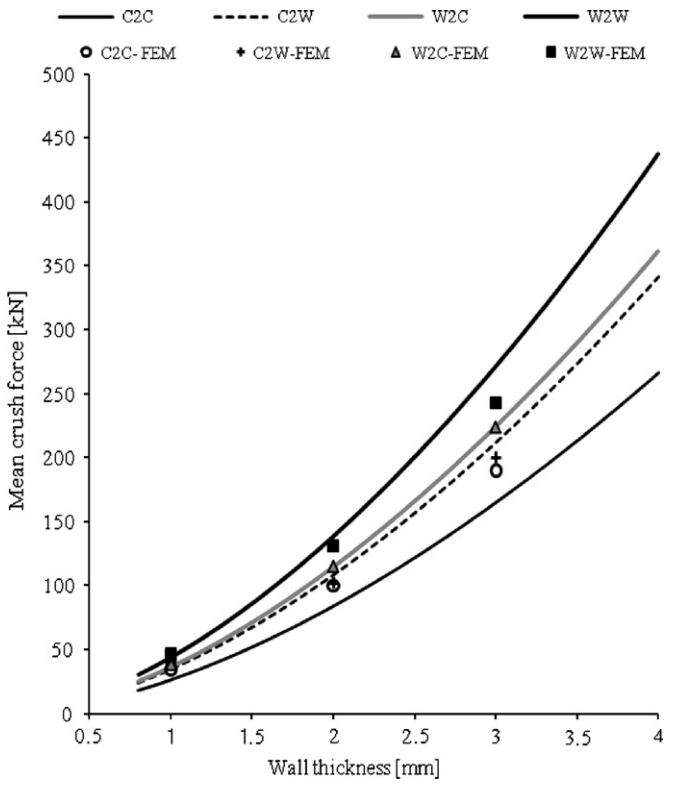

Fig. 16. Comparison of the analytical and FEA predictions of the mean crush force for different thicknesses.

simulation results for three different thickness values are also shown for comparison. Very close agreement is seen between the results in these cases. As discussed earlier, the analytical equation is valid as long as the mode of deformation does not change. Crush mode is mainly dependent on the trigger mechanism and wall thickness as opposed to the flange size or C/t ratio. This puts a limitation on the analytical equation, and in the case of altering crush modes, the analytical equation needs to be revised.

The average value for the equivalent projected fold length H from FE simulations is compared with the H_{eq} from Eq. (15) in Table 4. The results differ within 1–17%.

The assumptions and approaches used for the energy absorption characterization of multi-cell tubes based on FEA and the analytical procedure are listed in Table 5.

As noted earlier, the value of mean crush force in analytical equation is highly dependent upon the proper selection of the effective crush distance and energy equivalent flow stress. The effect of χ parameter for C2C configuration within the range of 0.6–0.75 is plotted in Fig. 17. This behavior has been observed for

Table 4
Comparison of equivalent projected fold length (H) for multi-cell, multi-corner tube models.

	H_{eq} (mm)	
	Eq. (15)	FEA
C2C	10.8	10.6
C2W	7.3	6.3
W2C	8.8	9.7
W2W	4.9	5.8

Table 5
Comparison between finite element simulation and analytical method for energy absorption characterization.

	FEA	SFE
Material behavior	Material is modeled using piecewise linear isotropic hardening with J_2 plasticity	Material is modeled using energy equivalent flow stress with rigid-perfectly plastic model
Kinematics	Kinematic of deformation is predicted from solving differential equations based on defined shape function within each element	Kinematic of deformation needs to be known based on experimental observation or simulation of deformation history
Energy dissipation	Calculated in each element based on the actual stress–strain behavior Integration points consider the stress distribution through shell thickness First-order shear deformation theory is used with shear correction factor of 0.833	Calculated based on the defined kinematics and single value of energy equivalent flow stress
Lobe contact	Imposed by penalty algorithm as a constraint on the element penetration	Is modeled by defining the effective crush distance
Crush force	Contact force	Directly from the energy balance equation
Crush distance	Predicted by the stroke advancement	Assigned by the effective crush distance
Solution	Nonlinear explicit solution of the governing equation Implicit solver for plasticity model	Algebraic analytic solution
Error sources	Round off, hourglass, element density, element distortion, material model	Averaging kinematic parameters H_{eq} and b_{eq}, energy equivalent flow stress Non-uniform distribution of strain is ignored The effective crush distance may vary in each configuration
Capability	Ability to model the actual boundary value problem, crush mode identification, dynamic and quasi-static	Rapid evaluation of design concepts Deeper understanding of the mechanism of energy dissipation

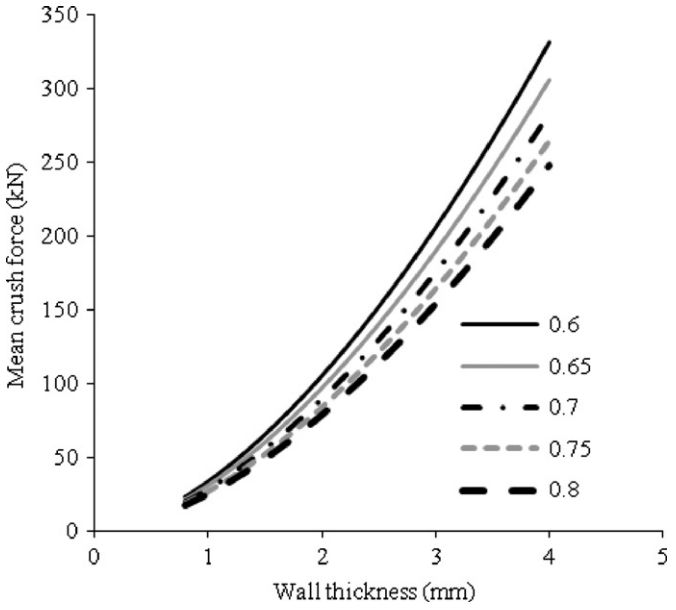

Fig. 17. Effect of parameter χ on the mean crush force for C2C configuration.

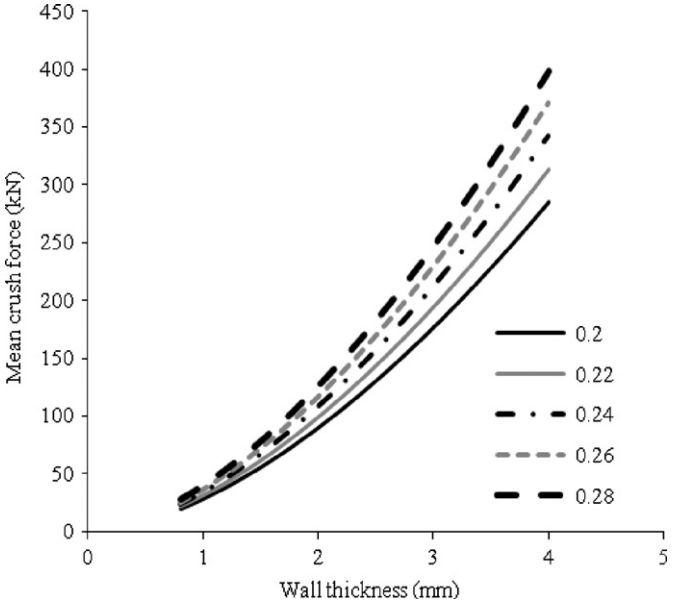

Fig. 18. Effect of energy equivalent flow stress on the mean crush force for C2W configuration.

all configurations. As the thickness increases, the effect of χ becomes more significant.

The effect of the uniform energy equivalent flow stress on the mean crush force of C2W configuration is shown in Fig. 18. Similar to the influence of effective crush distance due to the linear relationship between mean crush force and energy equivalent flow stress, increasing the thickness increases the difference between mean crush force predictions.

The calculation of mean crush force is found to depend greatly on the proper selection of effective crush distance and energy equivalent flow stress. However, specifying a proper effective crush distance becomes difficult in multi-cell tubes. Energy-equivalent flow stress can be specified more accurately by identification of strain in each separate localized region.

For comparison with the analytical model $P_m = (2/3)\sigma_0 t\sqrt{\pi m A}$ in Chen and Wierzbicki [8], model W2W is divided into m separate flanges with the material cross-sectional area denoted as A. For the model $P_m = \sigma_0 t\sqrt{(N_1+2N_2+2N_3)\pi t L_c}$ in Zhang et al. [25], the number of two-flange elements is denoted by N_1 and three-flanges as N_2 (for T-shape). It is worth noting that the flow stress in Zhang et al. [25] is derived from $\sigma_o = \sqrt{\sigma_y \sigma_u/(1+n)}$, where σ_y and σ_u represent the yield strength and ultimate strength of the material, respectively, with n as the exponent of the power law, which may underestimate the actual energy equivalent flow stress of the material. They also mention that it is required to use a dynamic correction factor of 1.2–1.4, which may not be appropriate in the presence of asymmetric trigger mechanism and the rate independent material. Chen and Wierzbicki [8] and Zhang and Cheng [10] studied the performance of multi-cell tubes for energy absorption. The main feature of the multi-cell tubes they considered was that they have equal-sized cells with right angle corners. In Table 6, the simulation-based results for average crush force are compared with the analytical predictions for the W2W configuration. The predicted values based on the analytical models in Chen and Wierzbicki [8] and Zhang et al. [25] are also shown for comparison.

Table 6
Comparison of the analytical and FEA predictions of the mean crush force for W2W model.

	Chen and Wierzbicki [8]	Zhang et al [25]	Present study	FE simulation
P_m (kN)	120	105	136	131
P_m-difference (%)	8.4	19.9	3.8	N/A
H_{eq} (mm)	9.4	8.6	4.9	5.8
H_{eq}-difference (%)	62.1	48.3	15.5	N/A

5. Conclusions

The energy absorption behavior of thin-walled, multi-corner tubes under axial compression was investigated using both numerical and analytical approaches. The effect of cross-sectional geometry on energy absorption was studied by analyzing several multi-cell, multi-corner tube models. The geometric features of interest included the arrangement of the interior tube walls and their connectivity with the exterior tube walls that resulted in acute or obtuse angles.

FE simulation results showed that the multi-cell tubes have less crush force fluctuation than a single-cell tube of equal mean crush force. Detailed evaluation of crush mode and folding length in each wall showed a complex deformation pattern in multi-cell, multi-corner configurations due to different corner angles, number of webs connected at each corner and the size of each web. The actual and projected fold lengths were different because of these factors.

The analytical method developed here was found to be highly dependent on the accurate mathematical description of kinematically admissible deformation that, as indicated by FE simulation results, can change due to the existence and the type of trigger mechanism used. Plastic work in each localized region was defined based on the uni-axial stress that was dominant in each region. As was observed in the FE simulation results obtained here and the experimental observations reported in the literature, dynamic loading can change the crush behavior of multi-corner tubes. To include the effect of strain rate sensitivity in the analytical equation, the mode of deformation must remain the same.

The comparison between the mean crush force of multi-cell tubes found from the analytical equation and that based on FE simulation showed a very good agreement. The analytical model was also able to predict the trend in mean crush force for different

thicknesses and different cross-sectional configurations. A sensitivity analysis on two major parameters including energy-equivalent flow stress and effective crush distance showed that the mean crush force is highly sensitive to changes in these two parameters, which can vary in different cross-sectional geometries. Similar to kinematically admissible deformation, these parameters should be assigned a priori as they cannot be determined from the solution.

Acknowledgements

The funding provided for this study by the US Department of Energy under Grant No. DE-FC26-06NT42755 is gratefully acknowledged.

References

[1] Chung TE, Lee YR, Kim CS, Kim HS. Design of aluminum space frame for crashworthiness improvement. SAE International 1996:960167.
[2] Alexander JM. An approximate analysis of the collapse of thin cylindrical shells under axial loading. The Quarterly Journal of Mechanics and Applied Mathematics 1960;13(1):10–5.
[3] Wierzbicki T, Abramowicz W. On the crushing mechanics of thin walled structures. Journal of Applied Mechanics 1983;50:727–34.
[4] Abramowicz W, Jones N. Dynamic axial crushing of square tubes. International Journal of Impact Engineering 1984;2(2):179–208.
[5] Abramowicz W, Wierzbicki T. Axial crushing of multicorner sheet metal columns. Journal of Applied Mechanics 1989;56:113–20.
[6] Wierzbicki T, Abramowicz W. The mechanics of deep plastic collapse of thin walled structures. In: Jones N, Wierzbicki T, editors. Structural failure. New York: Wiley; 1989. p. 281–329.
[7] Abramowicz W. Thin-walled structures as impact energy absorbers. Thin-Walled Structures 2003;41(2–3):91–107.
[8] Chen W, Wierzbicki T. Relative merits of single-cell, multi-cell and foam-filled thin-walled structures in energy absorption. Thin-Walled Structures 2001;39(4):287–306.
[9] Kim HS. New extruded multi-cell aluminum profile for maximum crash energy absorption and weight efficiency. Thin-Walled Structures 2002;40(4):311–27.
[10] Zhang X, Cheng G. A comparative study of energy absorption characteristics of foam-filled and multi-cell square columns. International Journal of Impact Engineering 2007;34(11):1739–52.
[11] Langseth M, Hopperstad OS. Static and dynamic axial crushing of square thin-walled aluminum extrusions. International Journal of Impact Engineering 1996;18(7–8):949–68.
[12] DiPaolo BP, Monteirob PJM, Gronsky R. Quasi-Static axial crush response of a thin-wall, stainless steel box component. International Journal of Solids and Structures 2004;41(14):3707–33.
[13] DiPaolo BP, Tom JG. A study on an axial crush configuration response of thin-wall, steel box components : the quasi-static experiments. International Journal of Solids and Structures 2006;43(25–26):7752–75.
[14] Wierzbicki T, Recke L, Abramowicz W, Gholami T. Stress profiles in thin-walled prismatic columns subjected to crush loading, part I, compression. Computers and Structures 1994;51(6):635–41.
[15] Wierzbicki T, Recke L, Abramowicz W, Gholami T. Stress profiles in thin-walled prismatic columns subjected to crush loading, part II, bending. Computers and Structures 1994;51(6):635–41.
[16] Otubushin A. Detailed validation of a non-linear finite element code using dynamic axial crushing of a square tube. International Journal of Impact Engineering 1998;21(5):349–68.
[17] Faruque O, Saha N. Extruded aluminum crash can topology for maximizing specific energy abdorption. SAE Technical Paper Series; 2008.
[18] Najafi, A, Rais-Rohani, M. Influence of cross-sectional geometry on crash characteristics of multi-cell prismatic columns. In: Proceedings of the 49th AIAA/ASME/ASC/AHS/ASC structures, structural dynamics and materials conference, Schaumburg, IL, 2008.
[19] Belytschko T, Liu WK, Moran B. Nonlinear finite elements for continua and structures. New York: John Wiley & Sons; 2000.
[20] Hughes, TJR. Nonlinear dynamic finite element analysis of shells, nonlinear finite element analysis in structural mechanics. In: Proceedings of the Europe–U.S. workshop, Ruhr-Universitat Bochum, Germany, 1981. p. 151–68.
[21] Hughes TJR. Finite element method—linear static and dynamic finite element analysis. Englewood Cliffs: Prentice-Hall; 2000.
[22] Belytschko T, Neal MO. Contact-impact by the pinball algorithm with penalty projection and Lagrangian methods. International Journal of Numerical Methods in Engineering 1991;31:547–72.
[23] Wriggers P. Computational contact mechanics. Wiley; 2002.
[24] Simo JC, Hughes TJR. Computational inelasticity. New York: Springer; 2000.
[25] Zhang X, Cheng G, Zhang H. Theoretical prediction and numerical simulation of multi-cell square thin-walled structures. Thin-Walled Structures 2006;44(11):1185–91.
[26] Santosa, SP. Crash behavior of box columns filled with aluminum honeycomb or foam. Master's thesis, Mechanical Engineering. Cambridge, MA: MIT; 1997.
[27] Santosa, SP. Crashworthiness analysis of ultralight metal structures. Ph.D. dissertation, Mechanical Engineering. Cambridge, MA: MIT; 1999.
[28] Bi, J, Fang, H, Wang, Q, Park, JW. Crashworthiness optimization of foam-filled thin-walled structures. In: Proceedings of the 49th AIAA/ASME/ASC/AHS/ASC structures, structural dynamics and materials conference, Schaumburg, IL, 2008.
[29] Hou S, Li Q, Long S, Yang X, Li W. Design optimization of regular hexagonal thin-walled columns with crashworthiness criteria. Finite Elements in Analysis and Design 2007;43(6—7):555–65.
[30] de Kanter, JLCG. Energy absorption of monolithic and fiber reinforced aluminum cylinders. PhD dissertation, Delft University of Technology (TUDelft), The Netherlands, 2006.
[31] Halquist J. LS-DYNA theoretical manual. Livermore Software Technology Corporation; 1998.
[32] Halquist J. LS-DYNA user's manual version 971. Livermore Software Technology Corporation; 2006.
[33] Abramowicz W. The effective crushing distance in axially compressed thin-walled metal columns. International Journal of Impact Engineering 1983;1(3):309–17.
[34] Abramowicz W. Extermal paths in progressive plasticity. International Journal of Impact Engineering 1996;18(7–8):753–64.
[35] Lu G, Tongxi Y. Energy absorption of structures and materials. Woodhead Publishing; 2003.
[36] Hayduk RJ, Wierzbicki T. Extensional collapse modes of structural members. Computers and Structures 1984;18(3):447–58.
[37] Wierzbicki T, Schneider F. Energy equivalent flow stress in crash calculations. Impact and Crashworthness Laboratory, MIT; 1999.
[38] Hill R. The mathematical theory of plasticity. Oxford University Press; 1998.
[39] Abramowicz, W. Crush resistance of 'T' 'Y' and 'X' sections. Joint MIT-Industry Program on Tanker Safety, Report No. 24, January 1994.